Electronic Supplementary Material (ESI) for Biomaterials Science.
This journal is © The Royal Society of Chemistry 2021

Supporting Information

DNase I Functional Microgels for Neutrophil Extracellular Trap Disruption

*Aisa Hosseinnejad[1], Nadine Ludwig[2], Ann-Katrin Wienkamp[2], Rahul Rimal[1], Christian Bleilevens[3], Rolf Rossaint[3], Jan Rossaint[2], Smriti Singh[1,4]**

A. Hosseinnejad, R. Rimal, Dr. S. Singh
[1] DWI—Leibniz-Institute for Interactive Materials e.V.
Forckenbeckstr. 50, 52056 Aachen, Germany

Prof. Dr. J. Rossaint, N. Ludwig, A. K. Wienkamp
[2] Department of Anesthesiology, Intensive Care and Pain Medicine, University Hospital Münster, Albert-Schweitzer-Campus 1, Bldg. A1, 48149 Münster, Germany

PD Dr. Christian Bleilevens, Prof. R. Rossaint
[3] The Department of Anaesthesiology of the University Hospital RWTH Aachen
Pauwelsstraße 30, 52074 Aachen, Germany

Dr. S. Singh
[4] Max-Planck-Institut für medizinische Forschung
Jahnstraße 29, 69120 Heidelberg, Germany
smriti.singh@mr.mpg.de

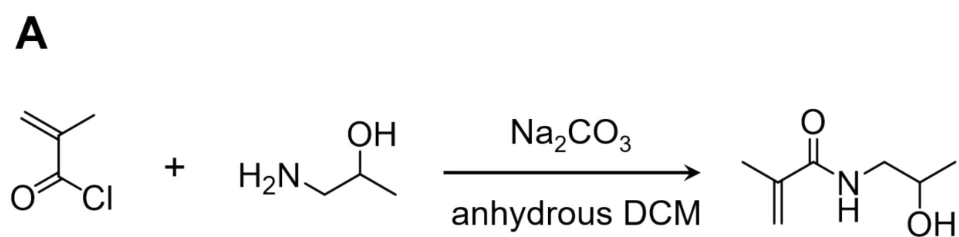

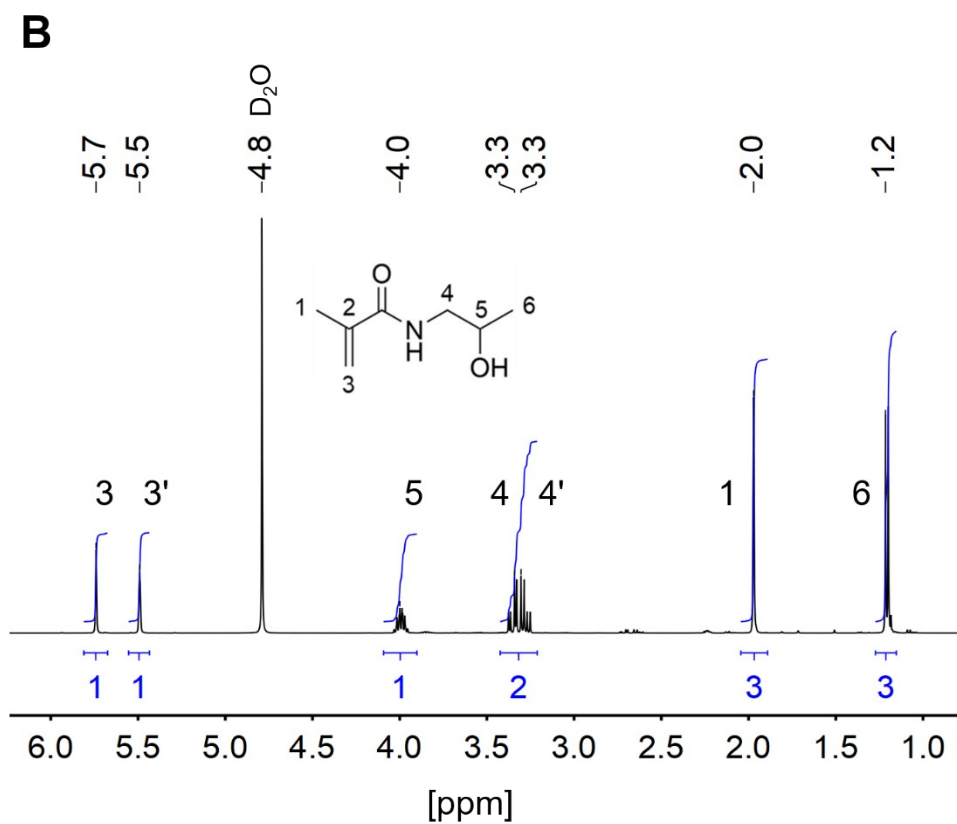

Figure S1. (A) Synthesis route and **(B)** ^{1}H NMR (300 MHz, D_2O) of HPMA.

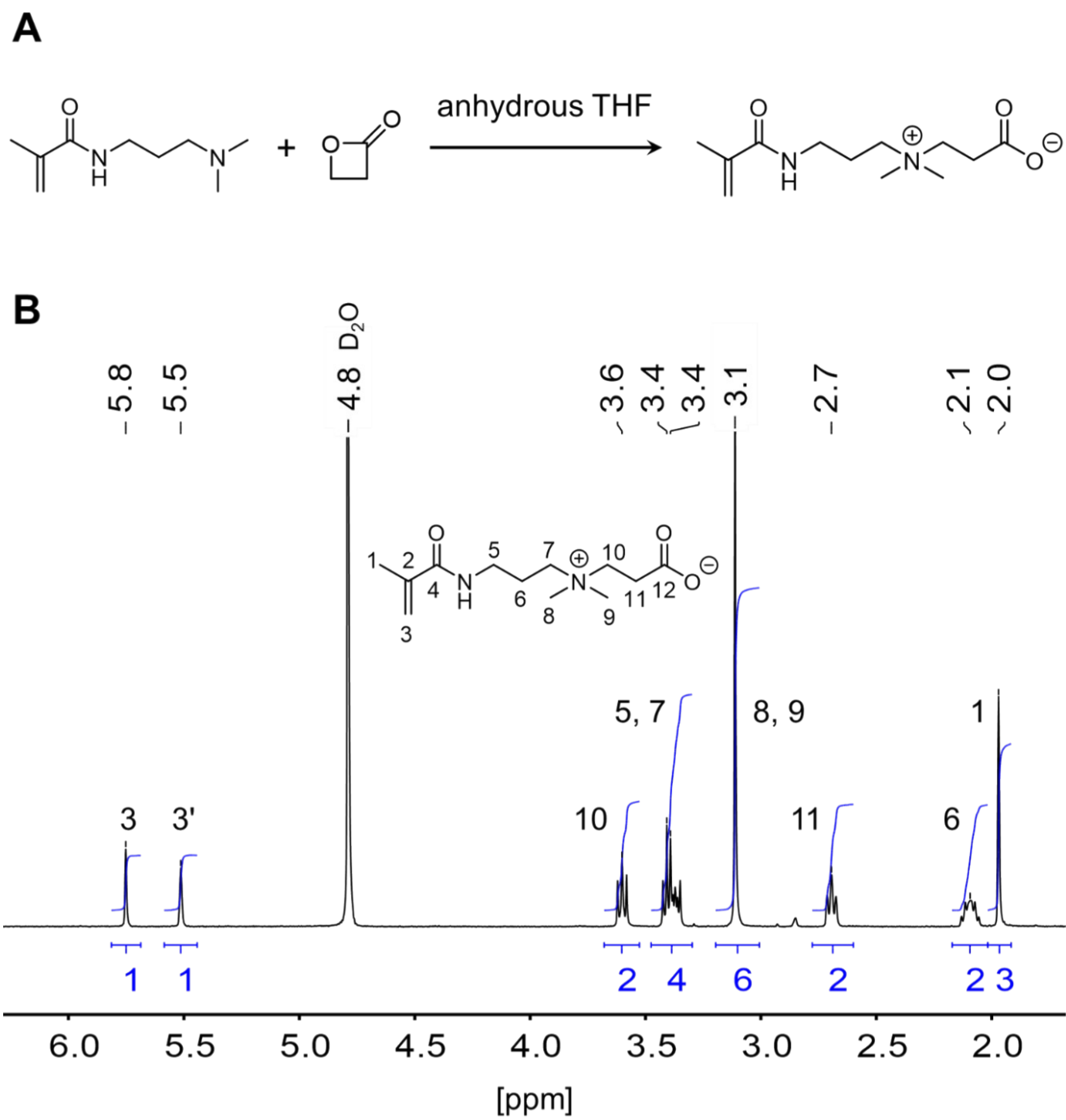

Figure S2. ^{1}H NMR (D_2O) of CBMAA from the inset synthesis route.

Table S1. Optimal parameters of the miniemulsion

aqueous phase	organic phase	volume ratio	surfactants	weight ratio of the surfactant mixture
PBS	Hexadecane	1:10	Span 80 (HLB = 4.3) Tween 80 (HLB =15)	Span 80: Tween 80 3:1 (HLB = 7)

monomer		crosslinker		initiator	
HPMA CBMAA	80 mol% 14 mol%	MBAA	3 mol% 6 mol% 8 mol% 10 mol%	AMPA	3 mol%

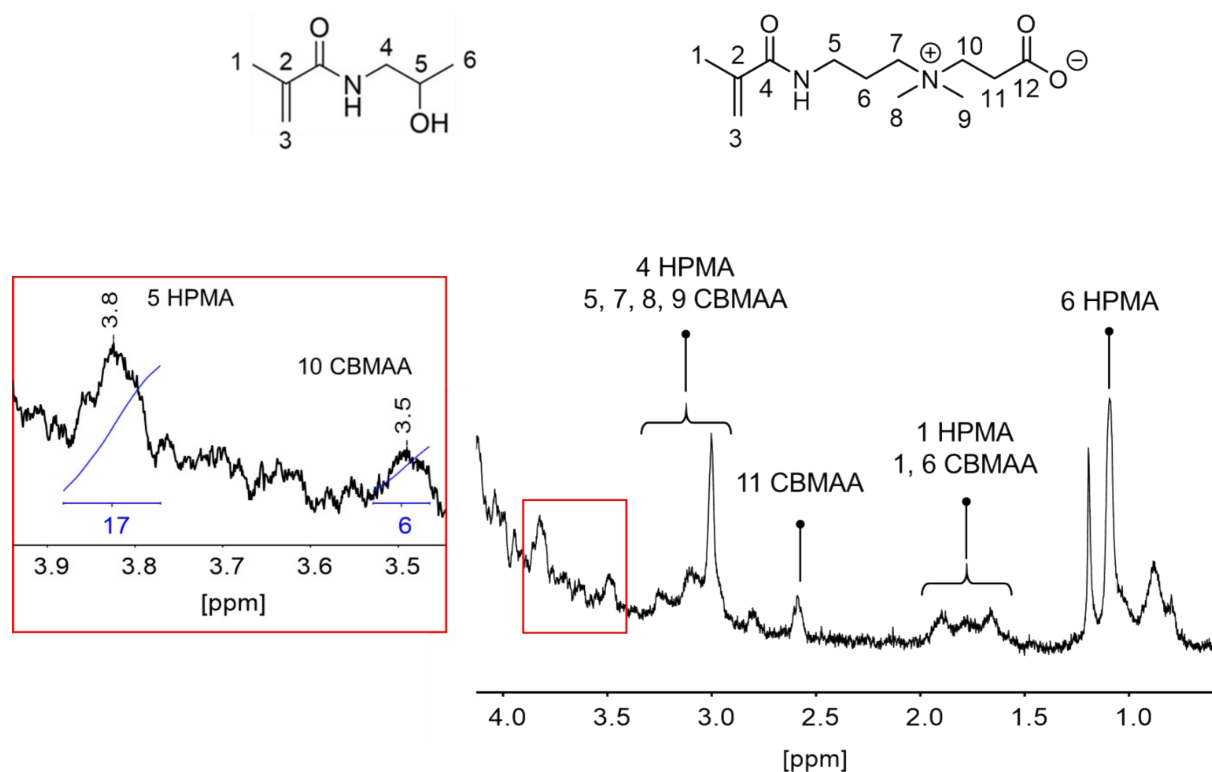

Figure S3. ^{1}H NMR of p(HPMA-*co*-CBMAA) microgels indicating the characteristic peaks. The inset shows the molar ratio of HPMA:CBMAA as set in the feed.

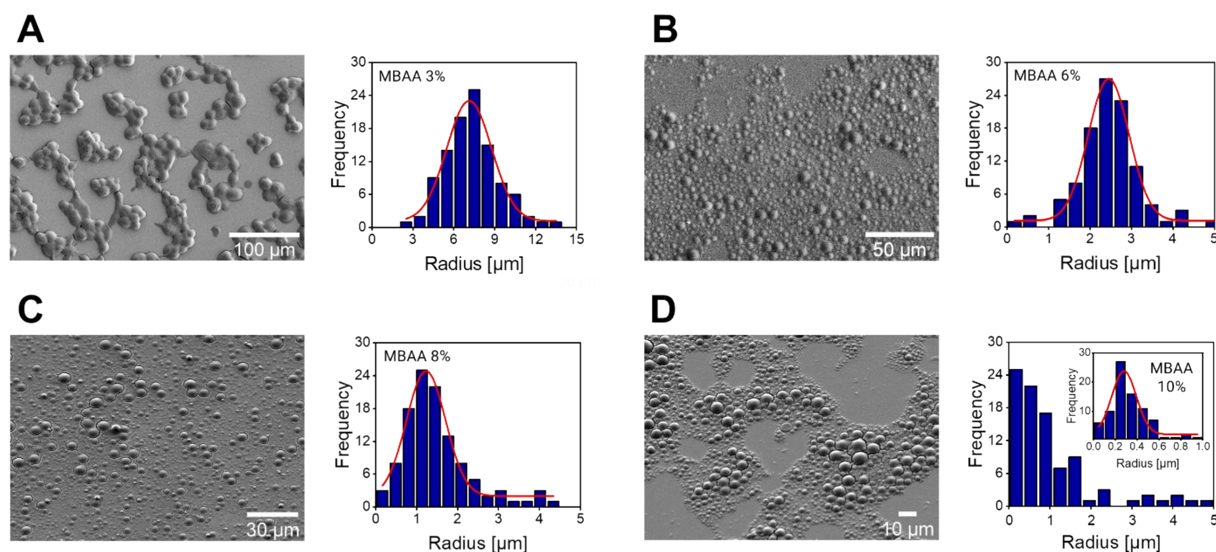

Figure S4. SEM and size distribution of microgels respecting the increase of crosslinker concentration in mmol%: **(A)** 3% MBAA, **(B)** 6%, MBAA, **(C)** 8% MBAA, **(D)** 10% MBAA (The size distribution inset shows that the microgels with size below 1 µm are the major population). Particle diameter was measured by ImageJ software using the given SEM images. The frequency distribution of particle size was plotted with Origin software. X-axis represents the particle radius in micrometer, while y-axis represents particle counts at a given radius. The red fitting curve shows the Gaussian distribution of the microgels.

Table S2. Summary table from the measurement of the particle size distribution including the average radius (R) and particle counts (N) for each microgel preparation with respect to the amount of crosslinker.

	MBAA 3%	**MBAA 6%**	**MBAA 8%**	**MBAA 10%**
Size [R, µm]	7.1 ± 1.6	2.5 ± 0.5	1.2 ± 0.5	0.3 ± 0.1
N	104	104	113	82

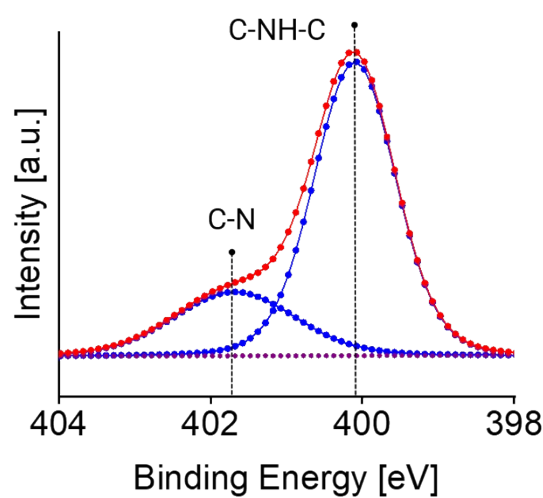

Figure S5. High resolution N 1s XPS spectra of native DNase I showing the characteristic structural peaks.

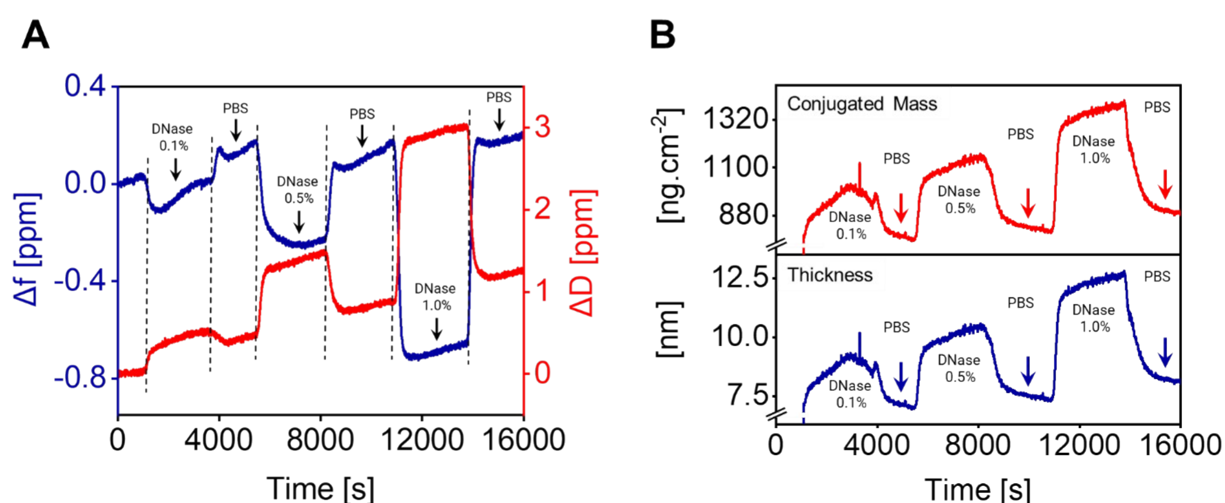

Figure S6. (A) The antifouling assay of EDC/sulfo-NHS activated p(HPMA-*co*-CBMAA) microgels against different concentrations of DNase I solutions (0.1, 0.5, 1.0 wt% in PBS pH 7.4) evaluated by a long-term QCM-D measurement. The results show oscillating changes of frequency (blue) and energy dissipation (red) by alternating the use of DNase I solution and PBS (pH 7.4). **(B)** Modeled QCM-D data for the representation of conjugated mass (red) and layer thickness (blue) on the quartz sensor.

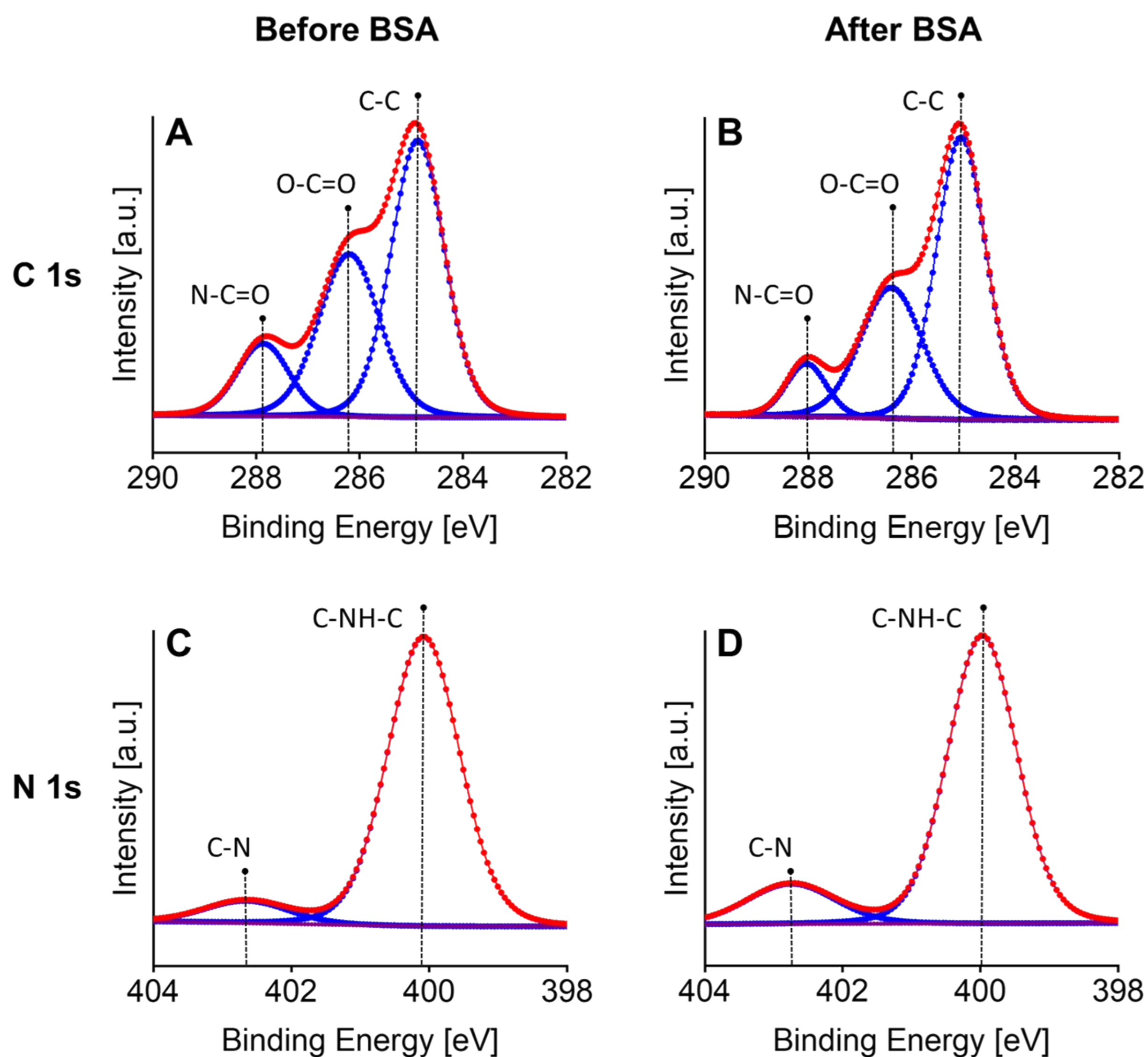

Figure S7. High resolution C 1s and N 1s XPS spectra of the DNase I microgels showing the characteristic structural peaks respectively **(A, C)** before and **(B, D)** after exposure to BSA.

Table S3. Elemental composition of microgels before and after BSA

	C 1s	**N 1s**	**O 1s**
Before BSA	51.5 ± 1.3 %	9.8 ± 1.4 %	38.7 ± 0.3 %
After BSA	51.3 ± 0.4 %	10.1 ± 0.9 %	38.6 ± 0.5 %

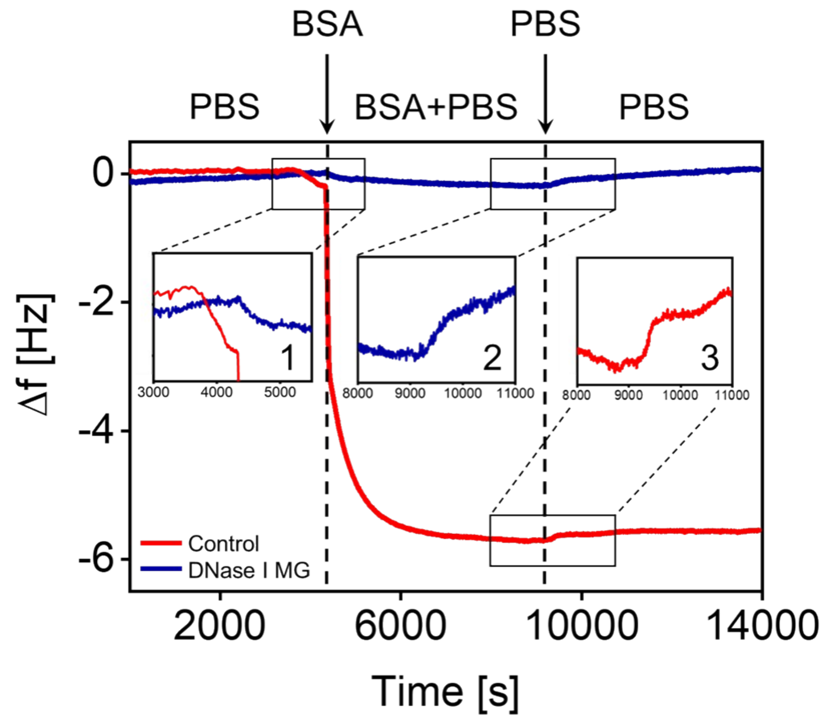

Figure S8. The antifouling assay of DNase I MGs coated on a gold sensor and a bare gold surface as a control by a long-term QCM-D measurement. The results show oscillating changes of frequency by addition of 0.01% BSA (in PBS pH 5.0) followed by a washing step using PBS (pH 5.0).

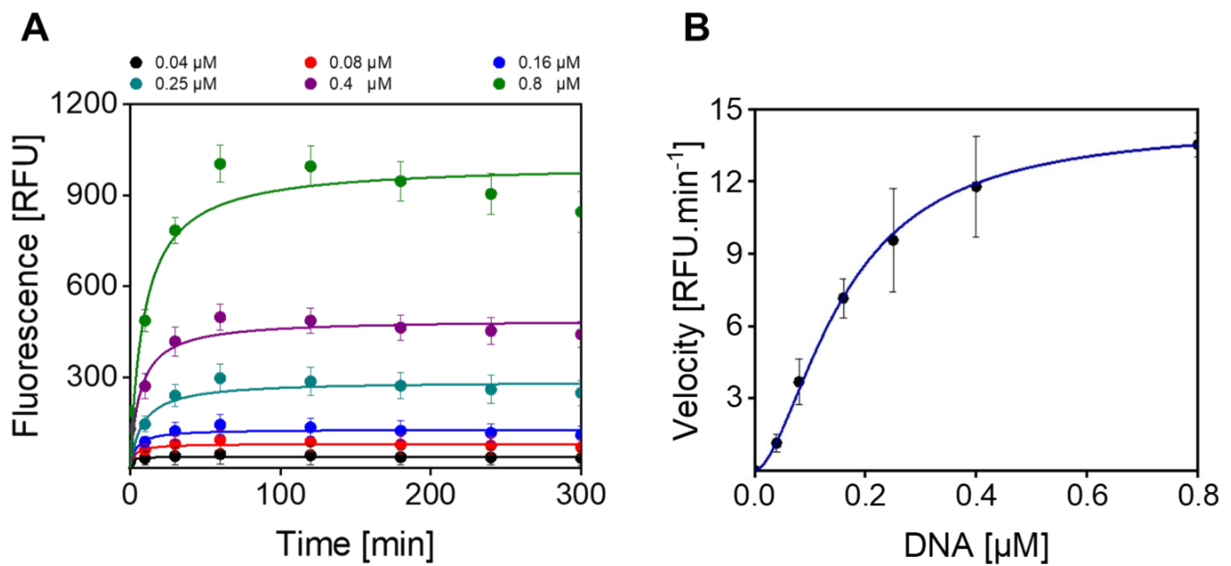

Figure S9. (A) Quantitative analysis of free DNase I kinetics by measuring the fluorescence over time using different substrate concentrations. Reactions contained 8 μM of the free enzyme. Fluorescence was normalized by subtraction of background fluorescence observed in the absence of enzyme. **(B)** The velocity data were fitted to the Hill model by non-linear regression and V_{max} and K_{Hill} were calculated to be 14.34001 ± 0.186 and 0.15945 ± 0.006 μM respectively. The error bars represent the standard error of the regression (n=3-4).

To estimate the enzymatic activity 8 μM of free DNase I was used. The concentration of free DNase used was equivalent to the immobilized DNase in 1 mg mL^{-1} of the DNase I MG. The changes in fluorescence intensity were recorded for 5 hr at 37 °C after incubation of free DNase I with different concentrations of the model DNA substrate. As shown in **Figure S9A** the fluorescence intensity over time was increased with the increase in concentration of the substrate. A plateau was attained after a full cleavage at a substrate concentration of 0.8 μM making the substrate concentration rate-limiting. The plot of velocity of the enzyme ($RFU \cdot min^{-1}$) as a function of the substrate concentration shows a sigmoidal curve contrary to the rectangular parabola given by Michaelis-Menten kinetics. Such sigmoidal curve shows cooperative binding of the enzyme.[14] Using Hill equation V_{max} and K_{Hill} of DNase I was calculated to be 14.34001 ± 0.186 and 0.15945 ± 0.006 μM respectively.

Video S1. Stimulated PMNs using phorbol 12-myristate13-acetate (PMA) to produce NETs.

Video S2. Stimulated PMNs in presence of the DNase I MGs. The disappearance of the orange spots shows the digestion of released NETs by the DNAse I MGs.

Video S3. Unstimulated PMNs in presence of the DNase I MGs. The orange spots show the expelled NETs staining with the cell impermeable DNA dye SYTOX™ orange.

Video S4. Unstimulated PMNs as a control group indicating the characteristic shape with Hoechst blue staining of the nuclei.